A spatial light modulator for terahertz beams

Wai Lam Chan,[1] Hou-Tong Chen,[2] Antoinette J. Taylor,[2] Igal Brener,[3] Michael J. Cich,[4] and Daniel M. Mittleman[1,a)]

[1]*Department of Electrical and Computer Engineering, Rice University, MS 366, Houston, Texas 77251-1892, USA*
[2]*Los Alamos National Laboratory, Center for Integrated Nanotechnologies, P.O. Box 1663, MS K771, Los Alamos, New Mexico 87545, USA*
[3]*Sandia National Laboratories, Center for Integrated Nanotechnologies, P.O. Box 5800, MS 1082, Albuquerque, New Mexico 87185, USA*
[4]*Sandia National Laboratories, MS 1082, Albuquerque, New Mexico 87185, USA*

(Received 3 April 2009; accepted 11 May 2009; published online 28 May 2009)

We design and implement a multipixel spatial modulator for terahertz beams using active terahertz metamaterials. Our first-generation device consists of a 4×4 pixel array, where each pixel is an array of subwavelength-sized split-ring resonator elements fabricated on a semiconductor substrate, and is independently controlled by applying an external voltage. Through terahertz transmission experiments, we show that the spatial modulator has a uniform modulation depth of around 40% across all pixels, and negligible crosstalk, at the resonant frequency. This device can operate under small voltage levels, at room temperature, with low power consumption and reasonably high switching speed. © *2009 American Institute of Physics*. [DOI: 10.1063/1.3147221]

Recent advances in terahertz technology and applications continuously drive the demand for novel terahertz devices. In the past decade, much research effort has been focused in the area of terahertz generation and detection,[1,2] while many functional devices for direct manipulation and processing of terahertz radiation are still lacking. One example is a spatial light modulator (SLM) for terahertz beams. SLMs allow the optical or electrical control of the spatial transmission (or reflection) of an input light beam, and thus the ability to redirect or encode information in a wave front. Such devices are key components for many optical and optoelectronic systems, with applications in optical processing, optical interconnections, image display, and real-time beam steering.[3,4] This technology, if extended to the terahertz region of the spectrum, can benefit exciting applications in terahertz imaging[5] and communications.[6,7] For instance, in a recent single-pixel terahertz imaging system,[5] a high-speed SLM is the crucial component for encoding random spatial patterns into the wave front of a terahertz beam.

The construction of a terahertz SLM requires an array of small terahertz devices that can independently control the transmission of a terahertz beam at their respective array positions. Traditional technologies for SLMs in the optical regime,[3,8] which use liquid crystals, magneto-optic effects, or deformable mirrors, do not operate efficiently in the terahertz regime because of the lack of materials with the desired terahertz response and/or the size mismatch between micromachined devices and terahertz wavelengths. Terahertz modulators based on quantum-well structures either require cryogenic cooling[9] or have a poor modulation depth.[10] Other previous efforts in building terahertz modulators also yield modulation of only a few percent[11] or require high operation voltage.[12]

In this letter, we report the construction of a terahertz SLM based on the use of active terahertz metamaterials.[13–16] This metamaterial device consists of a planar array of subwavelength-sized split-ring resonator (SRR) elements fabricated on epitaxial *n*-doped GaAs grown on a semi-insulating GaAs substrate[13] [see Figs. 1(a) and 1(b)]. The control of the metamaterial resonance is realized by the depletion of substrate charge carriers upon voltage bias which in turn changes the loss at the capacitive split gaps and therefore the oscillator strength of all of the individual SRR elements within a pixel. The device enables an amplitude

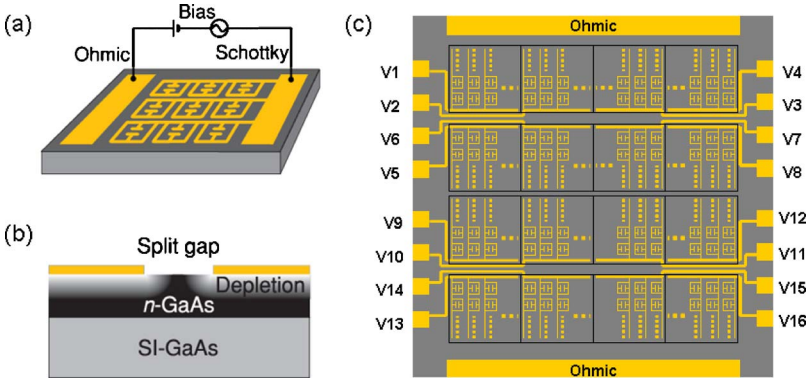

FIG. 1. (Color online) (a) Each single pixel on the terahertz SLM contains a 4×4 mm^2, 2500 element array of metamaterial SRRs. These elements are connected together with metal wires to serve as a metallic (Schottky) gate. An external voltage bias controls the substrate charge carrier density near the split gaps, tuning the strength of the resonance. (b) Diagram of the substrate and the depletion region near the split gap of a single SRR, where the gray scale indicates the free charge carrier density. (c) The terahertz SLM (not drawn to scale) is a 4×4 array of individual pixels in (a). Each pixel is independently controlled by an external voltage between the 1×1 mm^2 Schottky electric pad and the ohmic contact.

a)Author to whom correspondence should be addressed. Electronic mail: daniel@rice.edu.

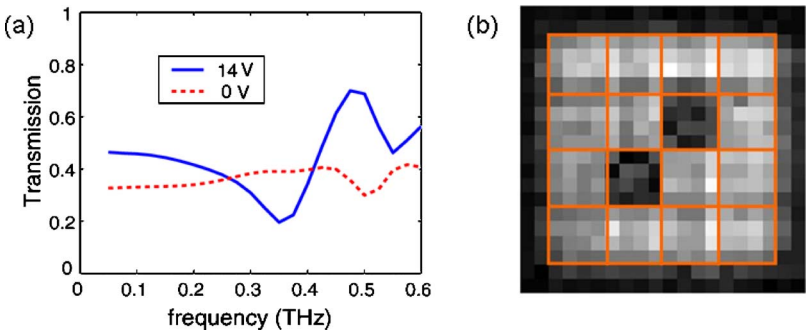

FIG. 2. (Color online) (a) Terahertz amplitude transmission spectra for one of the 16 pixels of the terahertz SLM without voltage bias (dashed) and with 14 V bias (solid). A large modulation depth is observed at 0.36 THz, the design resonant frequency. (b) A transmission image of the 4×4 array at 0.36 THz, with two pixels turned off (biased), and the rest turned on (zero bias).

modulation depth of ~3 dB under a relatively small bias voltage (16 V) at room temperature.[15] Moreover, fast modulation, in the megahertz range, is achievable.[14] The design of such metamaterial devices is flexible because the resonant frequency can be tuned by changing the geometry and dimensions of the SRR elements.[17] Compared to existing terahertz modulators,[9–12] the metamaterial-based devices are very promising for the construction of a high-speed terahertz SLM.

Our first demonstration of a terahertz SLM has 4 ×4 pixels, where each pixel is a 4×4 mm^2 array of metamaterial SRRs, as shown in Fig. 1(c). The SRR elements have 200 nm gold thickness, 4 μm line width, 2 μm split gap spacing, 66 μm outer dimension, and 76 μm period such that the device has a resonant transmission at 0.36 THz upon application of a voltage. Each pixel (consisting of 2500 SRRs) is independently controlled by an external voltage across a 1×1 mm^2 Schottky electric pad and the ohmic contact. This device has low power dissipation, drawing only a few milliamperes of current even when all the pixels are dc-biased at 14 V.

We characterize our terahertz SLM in a transmission geometry using a terahertz time-domain spectroscopy system with fiber-coupled photoconductive antennae for both terahertz generation and detection. The linearly polarized terahertz beam is collimated and directed toward the modulator with the polarization of the terahertz electric field aligned along the direction across the SRR split gaps. In these experiments, we raster-scan the terahertz receiver across the beam, after it has passed through the modulator. The substrate lens of the receiver antenna is covered by a metal mask with a 1 mm aperture to improve the spatial resolution of the measurement. At each receiver position, we measure the terahertz waveform using an optical chopper in the terahertz beam and a lock-in amplifier to filter the signal from the photoconductive antenna. Figure 2(a) shows the typical transmission spectra for one of the 16 pixels in the "on" and "off" configurations, i.e., under a dc bias voltage of 0 or 14 V, respectively. For all 16 pixels, we observe an amplitude modulation depth between 35% and 50% at the design resonant frequency of 0.36 THz. Shown in Fig. 2(b) is the transmission image of the 4×4 modulator array at 0.36 THz, with two pixels turned off (biased) and the rest turned on (zero bias).

To investigate the amount of crosstalk among the pixels in our terahertz SLM, we remove the optical chopper from the terahertz beam and instead modulate only certain pixel elements directly by applying a square-wave ac voltage bias, alternating between 0 and 14 V. Using a lock-in amplifier referenced to this square wave, we detect the terahertz signal at every receiver position of the raster-scan to produce a transmission image (Fig. 3 inset). Signals with the largest amplitudes are concentrated at the two modulated pixels, with only a small amount of crosstalk in the surrounding pixels. To measure system noise, we perform another raster-scan with all pixels unbiased and unmodulated (while the lock-in amplifier is still referenced to the square wave voltage frequency). From the first data set, for each frequency, we calculate $(N+C)/S$, the ratio of the signal power at the surrounding unmodulated pixels (due to both crosstalk C and noise N) to the signal power at the modulated pixel S (dotted curve in Fig. 3). We then calculate N/S, the ratio of the noise power from the second data set to S from the first data set (dashed curve). The difference between the two ratios gives the crosstalk level, independent of the system noise. This procedure is necessary because the crosstalk is so small as to be nearly indistinguishable from the noise.

As shown in Fig. 3, the crosstalk level (solid curve) is larger (−15 dB) at lower frequencies due to diffraction effects, but drops to around −30 dB near 0.33 THz. Above this frequency, quantifying the amount of crosstalk becomes challenging because the noise-to-signal ratio increases due to the decreasing terahertz spectral amplitude, making the crosstalk indistinguishable from system noise. As a result, this measurement is an upper limit on the crosstalk at the device operating frequency.

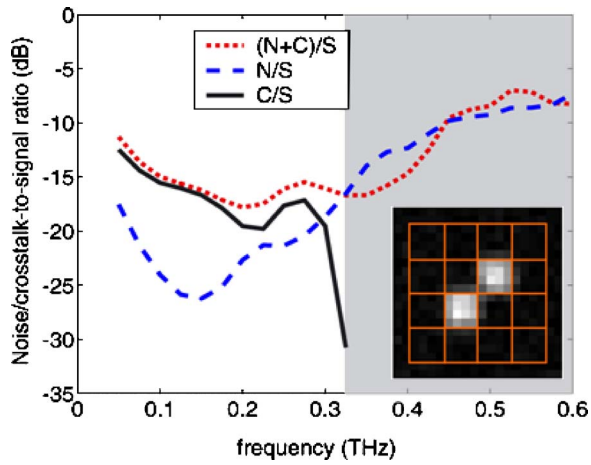

FIG. 3. (Color online) Noise-to-signal power ratio (dashed) and noise-plus-crosstalk-to-signal power ratio (dotted) across frequency, from which we obtain the crosstalk level (solid). Above 0.33 THz (in the shaded area), crosstalk is buried in noise, and is therefore unmeasurable. These ratios are calculated from their corresponding transmission images of the 4×4 array of the terahertz SLM at every frequency. In the inset image at 0.36 THz, two pixels are under a square voltage bias and the rest are unbiased. A terahertz modulation (differential) signal is measured at each pixel using the lock-in amplifier referenced to the square voltage.

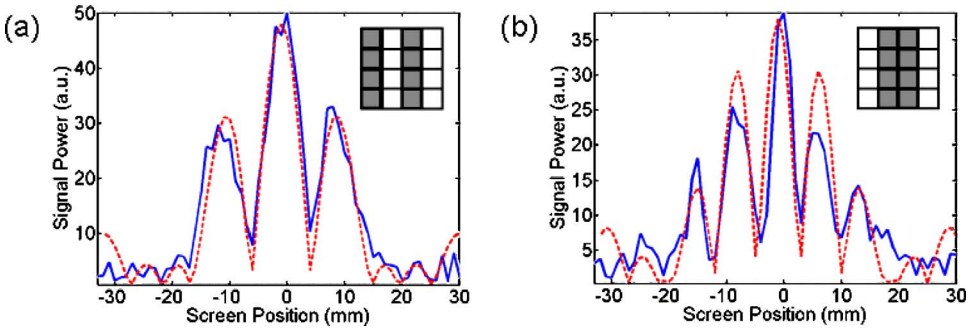

FIG. 4. (Color online) Measured (solid curves) differential fringe patterns produced by the transmission of the terahertz beam through the terahertz SLM in two double-slit configurations, compared with analytical calculations (dashed curves). The insets show the "on" and "off" configurations of the 16 pixels, with zero bias on the gray pixels, and the white pixels modulated with a 3 kHz square signal alternating between 0 and 14 V.

To provide an illustration of the dynamic switching capability of our terahertz SLM, we modulate certain pixel elements for two distinct configurations. Shown in the insets of Fig. 4 are two double-slit configurations. The white pixel elements are driven by a 3 kHz square wave varying between 0 and 14 V, which is also used as the reference for the lock-in amplifier. The array elements shown in gray are unbiased. We use a lens to focus the transmitted terahertz wave front, and the terahertz detector (with a 1 mm aperture) is scanned along a line in the focal plane of the lens, across a 64 mm interval. Figure 4 shows the measured differential fringe patterns (solid curves) at 0.36 THz for the two double-slit configurations. These have the same slit sizes ($b=4$ mm) but different slit separations [$a=8$ and 12 mm, respectively, in Figs. 4(a) and 4(b)]. As expected, the fringes appear at distances, multiples of $\lambda f/a$, away from the central fringe. Here, λ is the observation wavelength, f is the focal length of the focusing lens, and a is the slit separation. Analytical calculations of the double-slit diffraction pattern, assuming a plane wave illumination, best fit our measured data with $a=9.8$ and 13.8 mm, respectively, for the two configurations, and $b=5$ mm (see dashed curves in Fig. 4). When using metal slits of the same dimensions as those of the slits formed by the modulator in a direct observation of the diffraction fringes, we observe similar values for these fit parameters. This indicates that the differences between the fit parameters and the actual geometrical dimensions of the double slit are a result of the fact that the illuminating terahertz beam is not an ideal plane wave. To our knowledge, this is the first demonstration of fast dynamical modulation of a terahertz wave front.

To conclude, we have implemented the first electrical terahertz SLM based on metamaterial split-ring resonators. Our first-generation design, a 4×4 pixel array, demonstrates a high modulation depth at the resonant frequency, uniformly across all pixels, and a negligible amount of crosstalk among pixels. We demonstrate the kilohertz-rate operation of this spatial modulator by measuring a double-slit configuration to generate interference patterns. Our terahertz SLM operates at low voltages at room temperature and with low power consumption. Slight modifications can also achieve spatially varying phase modulation (instead of amplitude)[15] or dynamic tunability of the resonant frequency,[18] rendering numerous possible applications of this device design in future terahertz imaging and communication systems.

W.L.C. and D.M.M. acknowledge partial support from the National Science Foundation and from the Air Force Office of Scientific Research through the CONTACT program. H.T.C. and A.J.T. acknowledge support from the Los Alamos National Laboratory LDRD Program. This work was performed, in part, at the Center for Integrated Nanotechnologies, a US Department of Energy, Office of Basic Energy Sciences Nanoscale Science Research Center operated jointly by Los Alamos and Sandia National Laboratories. Los Alamos National Laboratory is operated by Los Alamos National Security, LLC under Contract No. DE-AC52-06NA25396, and Sandia is a multiprogram laboratory operated by Sandia Corporation, a Lockheed Martin Co., under Contract No. DE-AC04-94AL85000, for the National Nuclear Security Administration of the US Department of Energy.

[1] B. Ferguson and X.-C. Zhang, Nature Mater. **1**, 26 (2002).
[2] P. H. Siegel, IEEE Trans. Microwave Theory Tech. **50**, 910 (2002).
[3] U. Efron, *Spatial Light Modulator Technology: Materials, Devices and Applications* (CRC, Cleveland/Boca Raton, 1995).
[4] D. Engstrom, J. Bengtsson, E. Eriksson, and M. Goksor, Opt. Express **16**, 18275 (2008).
[5] W. L. Chan, K. Charan, D. Takhar, K. F. Kelly, R. G. Baraniuk, and D. M. Mittleman, Appl. Phys. Lett. **93**, 121105 (2008).
[6] T. Kleine-Ostmann, K. Pierz, G. Hein, P. Dawson, and M. Koch, Electron. Lett. **40**, 124 (2004).
[7] C. Jastrow, K. Munter, R. Piesiewicz, T. Kurner, M. Koch, and T. Kleine-Ostmann, Electron. Lett. **44**, 213 (2008).
[8] J. W. Goodman, *Introduction to Fourier Optics* (Roberts & Company, Greenwood Village, Colorado, 2004).
[9] R. Kersting, G. Strasser, and K. Unterrainer, Electron. Lett. **36**, 1156 (2000).
[10] I. H. Libon, S. Baumgartner, M. Hempel, N. E. Hecker, J. Feldmann, M. Koch, and P. Dawson, Appl. Phys. Lett. **76**, 2821 (2000).
[11] T. Kleine-Ostmann, P. Dawson, K. Pierz, G. Hein, and M. Koch, Appl. Phys. Lett. **84**, 3555 (2004).
[12] P. Kuzel, F. Kaldec, J. Petzelt, J. Schubert, and G. Panaitov, Appl. Phys. Lett. **91**, 232911 (2007).
[13] H.-T. Chen, W. J. Padilla, J. M. O. Zide, A. C. Gossard, A. J. Taylor, and R. D. Averitt, Nature (London) **444**, 597 (2006).
[14] H.-T. Chen, S. Palit, T. Tyler, C. M. Bingham, J. M. O. Zide, J. F. O'Hara, D. R. Smith, A. C. Gossard, R. D. Averitt, W. J. Padilla, N. M. Jokerst, and A. J. Taylor, Appl. Phys. Lett. **93**, 091117 (2008).
[15] H.-T. Chen, W. J. Padilla, M. J. Cich, A. K. Azad, R. D. Averitt, and A. J. Taylor, Nat. Photonics **3**, 148 (2009).
[16] O. Paul, C. Imhof, B. Lagel, S. Wolff, J. Heinrich, S. Hofling, A. Forchel, R. Zengerle, R. Beigang, and M. Rahm, Opt. Express **17**, 819 (2009).
[17] A. K. Azad, A. J. Taylor, E. Smirnova, and J. F. O'Hara, Appl. Phys. Lett. **92**, 011119 (2008).
[18] H.-T. Chen, J. F. O'Hara, A. K. Azad, A. J. Taylor, R. D. Averitt, D. B. Shrekenhamer, and W. J. Padilla, Nat. Photonics **2**, 295 (2008).